
INTERPOLATING NEURAL NETWORK: A LIGHTWEIGHT YET PRECISE ARCHITECTURE FOR DATA TRAINING, EQUATION SOLVING, AND PARAMETER CALIBRATION

Chanwook Park *

Department of Mechanical Engineering
Northwestern University
Evanston, IL 60208
chanwookpark2024@u.northwestern.edu

Sourav Saha *

Kevin T. Crofton Department of
Aerospace and Ocean Engineering
Virginia Polytechnic Institute
and State University
Blacksburg, VA 24060
sourav.saha@vt.edu

Jiachen Guo

Theoretical and Applied Mechanics Program
Northwestern University
Evanston, IL 60208
jiachenguo2020@u.northwestern.edu

Hantao Zhang

Theoretical and Applied Mechanics Program
Northwestern University
Evanston, IL 60208
hantaozhang2029@u.northwestern.edu

Xiaoyu Xie

Department of Mechanical Engineering
Northwestern University
Evanston, IL 60208
xiaoyuxie2020@u.northwestern.edu

Miguel A. Bessa

School of Engineering
Brown University
Providence, RI
miguel_bessa@brown.edu

Dong Qian

Department of Mechanical Engineering
University of Texas at Dallas
Richardson, TX 75080
dong.qian@utdallas.edu

Wei Chen

Department of Mechanical Engineering
Northwestern University
Evanston, IL 60208
weichen@northwestern.edu

Gregory J. Wagner

Department of Mechanical Engineering
Northwestern University
Evanston, IL 60208
gregory.wagner@northwestern.edu

Jian Cao

Department of Mechanical Engineering
Northwestern University
Evanston, IL 60208
j.cao@northwestern.edu

Wing Kam Liu †

Department of Mechanical Engineering
Northwestern University
Evanston, IL 60208
w-liu@northwestern.edu

November 18, 2024

*Equal contribution with Coauthor 1 and Coauthor 2

†Corresponding author

ABSTRACT

Artificial intelligence (AI) has revolutionized software development, shifting from task-specific codes (Software 1.0) to neural network-based approaches (Software 2.0). However, applying this transition in engineering software presents challenges, including low surrogate model accuracy, the curse of dimensionality in inverse design, and rising complexity in physical simulations. We introduce an interpolating neural network (INN), grounded in interpolation theory and tensor decomposition, to realize Engineering Software 2.0 by advancing data training, partial differential equation solving, and parameter calibration. INN offers orders of magnitude fewer trainable/solvable parameters for comparable model accuracy than traditional multi-layer perceptron (MLP) or physics-informed neural networks (PINN). Demonstrated in metal additive manufacturing, INN rapidly constructs an accurate surrogate model of Laser Powder Bed Fusion (L-PBF) heat transfer simulation, achieving sub-10-micrometer resolution for a 10 mm path in under 15 minutes on a single GPU. This makes a transformative step forward across all domains essential to engineering software.

1 Introduction

The evolution of software programming methodologies has transitioned from reliance on rigidly hard-coded instructions, governed by explicitly defined human rules, to the adoption of neural network-based algorithms. The transition is coined as "from *Software 1.0* to *Software 2.0*" [1]. The shift towards Software 2.0 partially resolved the issue of labor-intensive programming in Software 1.0 and has significantly advanced the domain of large language models (LLMs) and other foundational models [2, 3]. However, the application of these technologies in the fields of engineering and science presents unique challenges. One such challenge is the relatively low generalization accuracy of machine learning (ML)-based solvers compared to traditional numerical methods [4, 5, 6, 7, 8]. After in-depth research was conducted on those methods, an increasing number of researchers began to question their effectiveness [8, 9]. Another challenge is the curse of dimensionality that arises when solving inverse design problems. As the design parameter space grows, computation requirements easily become prohibitive. Furthermore, the complexity of physical simulations continues to increase. For instance, additive manufacturing (AM) or integrated circuit (IC) simulations necessitate extremely fine resolution with high accuracy and multi-physics/multi-scale analysis within a reasonable simulation time [10, 11, 12].

In this article, we propose the concept of *Engineering Software 2.0*, which aims to advance the current generation of computational and data-driven engineering software into a new paradigm.

"Engineering Software 2.0 is an end-to-end software system that unifies training, solving, and calibrating in science/engineering problems."

We introduce interpolating neural networks (INNs) to achieve the new paradigm of Engineering Software 2.0. The key ideas behind INNs are: 1) discretize an input domain into non-overlapping segments whose bounds are denoted by interpolation nodes, 2) construct a graph with the interpolation nodes and formulate the message passing operation as a form of interpolation functions, and 3) optimize the values and coordinates of the interpolation nodes for a given loss function. Figure 1 shows a pictorial description of the approach. When the input domain is discretized with a regular mesh (see the special case in Figure 1), an INN leverages tensor decomposition (TD) [13, 14, 15, 16] to convert the growth of the computational cost of a high-dimensional problem from exponential to linear. INN facilitates three major tasks in computational science and engineering: 1) trains on both experimental and simulation data with very high accuracy and minimal memory footprint, 2) solves high-dimensional parameterized partial differential equations (PDEs), and 3) calibrates uncertain parameters rapidly and accurately.

A representative application of INN can be found in metal additive manufacturing (AM), where a laser is used to melt and fuse metal powder to build a metal component layer by layer. As the laser spot size ranges from 50 to 100 μm [10, 17], physical simulations of AM require a sub-10 micron resolution that challenges most physical simulations [11, 18]. The required computational resources become prohibitive, particularly when they are employed to generate training data for a surrogate model within a vast parametric space. As illustrated in Figure 2, INN presents a new direction toward part-scale AM simulations for online manufacturing control, demonstrating performance gains by orders of magnitude. We also conduct various numerical experiments that cover computer science and engineering domains to demonstrate the superior capabilities of INN in training, solving, and calibrating. The computer codes can be found at <https://github.com/hachanook/pyinn>.

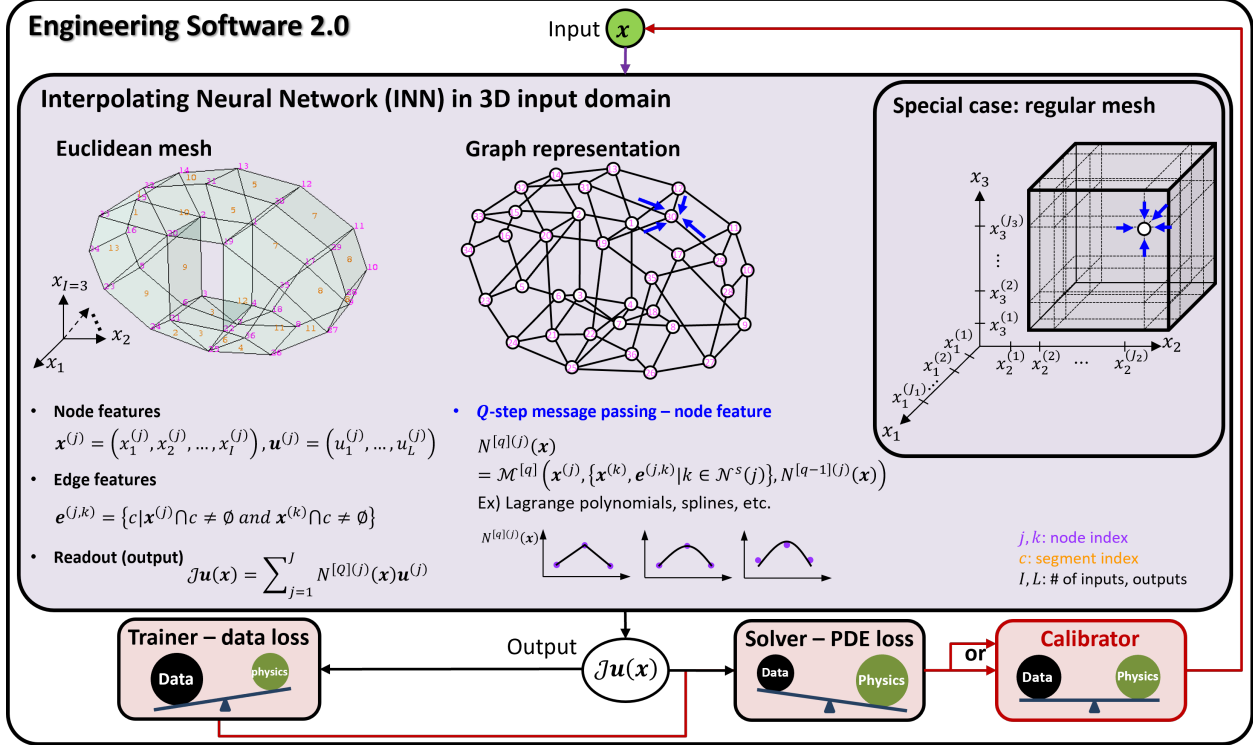


Figure 1: Overview of Engineering Software 2.0 enabled with Interpolating Neural Network (INN). The INN box illustrates the graph representation of the input domain discretized with an arbitrary Euclidean mesh (left) and a regular mesh as a special case (right). Node and edge features are given from the discretized mesh. After Q -step message passing, each node j will store an interpolation function $N^{[Q](j)}(\mathbf{x})$. Finally, the readout operation sums the product of the interpolation functions and nodal values $\mathbf{u}^{(j)}$. The superscripts with square brackets [] and parentheses () denote the message passing step and graph node index, respectively. The interpolation operator \mathcal{J} denotes that $\mathcal{J}\mathbf{u}(\mathbf{x})$ is a function that interpolates discrete values of $\mathbf{u}^{(j)}$. The INN trainer employs data-driven loss functions (e.g., mean squared error loss for regression) while the INN solver adopts a residual loss of a partial differential equation (PDE). A trained/solved INN model can then be employed as a forward model of a calibrator to solve an inverse problem.

2 INN: Unification of Training/Learning, Solving, and Calibrating

Interpolating Neural Network (INN) generalizes numerical methods such as the finite element method (FEM) [20, 21, 22] as a subset of deep neural network (DNN) via graph network operations. Although different groups of researchers have developed the two (FEM and DNN), they share one thing in common; the goal is to find a function. The former finds a solution field of a differential equation while the latter finds an input-output relationship. INN is built upon this similarity and forms the backbone of Engineering Software 2.0 that unifies training, solving, and calibrating, as illustrated in Figure 1.

Consider a regression problem that relates I inputs and L outputs. The first step of an INN is to discretize the input domain in the I -dimensional Euclidean space into a mesh, which can be as general as an unstructured irregular mesh or as specific as a structured regular mesh. In any case, a mesh in the Euclidean space can be readily represented as a graph – the most general form of a discretized input – as illustrated in the INN box of Figure 1. The conversion from mesh to graph has been widely accepted in the literature [23, 24, 25, 26]. Suppose there are J nodes (or vertices) and E edges in the graph, where the input domain is discretized with C non-overlapping segments. Each segment occupies a subspace of the I -dimensional input domain. For instance in Figure 1, the Euclidean mesh consists of segments of hexahedrons and triangular pillars.

Each node (e.g., node j) has two features: nodal coordinates ($\mathbf{x}^{(j)} \in \mathbb{R}^I$) and values ($\mathbf{u}^{(j)} \in \mathbb{R}^L$). Note that the superscript with parentheses refers to the graph node index. An edge that links node j and k has a feature $\mathbf{e}^{(j,k)}$ that stores indices of segments connected to the edge. For example, when $I = 3, L = 2$, node 10 in Figure 1 stores $\mathbf{x}^{(10)} = (x_1^{(10)}, x_2^{(10)}, x_3^{(10)})$ and $\mathbf{u}^{(10)} = (u_1^{(10)}, u_2^{(10)})$. The edge connecting nodes 30 and 12 stores $\mathbf{e}^{(30,12)} = \{5, 7\}$.

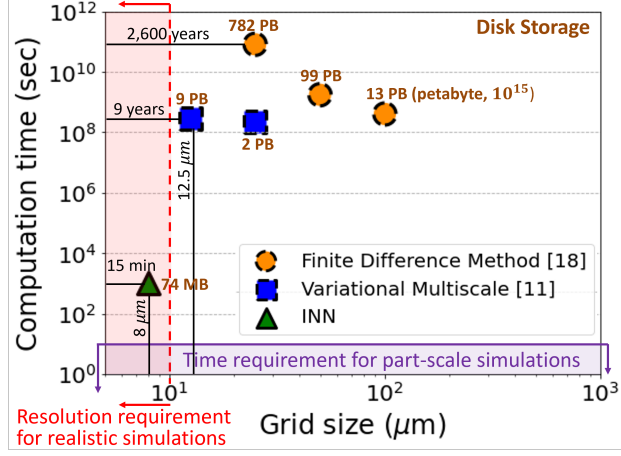


Figure 2: Benchmark comparison of the single-scale finite difference method (FDM) solver [18], the variational multiscale FEM solver [11], and the INN solver. The data points for the first two methods with dashed marker edges are estimated, while that of INN with a solid marker edge is computed. A 3D-space, time, and 4D-parameter heat transfer equation is solved to model a 10 mm single-track laser powder bed fusion (L-PBF) metal AM. Detailed problem definition and explanation can be found in Section 3. All solvers are graphics processing units (GPU) optimized with the JAX library [19].

A typical message passing in a graph neural network (GNN) returns a hidden state for each graph node which is mostly a tensor (including matrix and vector) [27]. In contrast, the INN message passing returns a function (i.e., interpolation function $N^{(j)}(\mathbf{x})$, or often called *shape function* in computational mechanics) for each node ($j = 1, \dots, J$) as a hidden state. A general Q -step message passing of an INN, $\mathcal{M}^{[q]}(*)$, can be expressed as:

$$N^{[q](j)}(\mathbf{x}) = \mathcal{M}^{[q]} \left(\mathbf{x}^{(j)}, \{\mathbf{x}^{(k)}, \mathbf{e}^{(j,k)} | k \in \mathcal{N}^s(j)\}, N^{[q-1](j)}(\mathbf{x}) \right), \quad q = 1, \dots, Q, \quad N^{[0](j)}(\mathbf{x}) = 0, \quad (1)$$

where $N^{[q](j)}(\mathbf{x})$ is the interpolation function at node j after q -th message passing and $\mathcal{N}^s(j)$ is a set of neighboring nodes of the center node j with s connections (i.e., s -hops, see Supplementary Information (SI) Section 1.1 for visual illustrations). It is worth noting that the interpolation functions satisfy the Kronecker delta property, i.e., $N^{[q](j)}(\mathbf{x}^{(k)}) = \delta_{jk}$. The operation $\mathcal{M}^{[q]}(*)$ constructs an interpolation function $N^{[q](j)}(\mathbf{x})$ for a graph node $\mathbf{x}^{(j)}$ using neighboring nodal coordinates and edge information: $\mathbf{x}^{(k)}, \mathbf{e}^{(j,k)}$, and the interpolation function of the previous message passing: $N^{[q-1](j)}(\mathbf{x})$. This can be any interpolation method such as Lagrange polynomials [28, 20], meshfree [29, 30, 31], and splines [32, 33]. The Q -step message passing implies that it is also possible to progressively construct nonlinear or more problem-specific interpolation functions, theoretically based on the generalized finite element method [34, 35] and convolution hierarchical deep learning neural networks [7, 15]. Depending on the choice of interpolation technique, other hyper-parameters can be involved in $\mathcal{M}^{[q]}(*)$ such as the activation (or basis) function and dilation parameter [7, 15]. See SI Section 1 for various choices of the message passing operation.

During the forward propagation, an input variable $\mathbf{x} \in \mathbb{R}^I$ enters each graph node's interpolation function $N^{[Q](j)}(\mathbf{x})$, followed by a graph-level readout operation:

$$\mathcal{J}\mathbf{u}(\mathbf{x}) = \sum_{j=1}^J N^{(j)}(\mathbf{x}) \mathbf{u}^{(j)}, \quad \mathbf{x} \in \mathbb{R}^I, \mathbf{u} \in \mathbb{R}^L, \quad (2)$$

where the superscript $[Q]$ is dropped for brevity (i.e., $N^{[Q](j)}(\mathbf{x}) = N^{(j)}(\mathbf{x})$). The interpolation operator \mathcal{J} will designate an interpolated field output throughout this paper. The readout operation can be written as a tensor contraction (or matrix multiplication):

$$\mathcal{J}\mathbf{u}(\mathbf{x}) = \begin{bmatrix} \mathbf{u}^{(1)} & \mathbf{u}^{(2)} & \cdots & \mathbf{u}^{(J)} \end{bmatrix} \cdot \begin{bmatrix} N^{(1)}(\mathbf{x}) \\ N^{(2)}(\mathbf{x}) \\ \vdots \\ N^{(J)}(\mathbf{x}) \end{bmatrix} = \mathbf{U} \times_2^1 \mathbf{\mathcal{X}}(\mathbf{x}) = \mathbf{U} \mathbf{\mathcal{X}}(\mathbf{x}), \quad (3)$$

where $\mathbf{u}^{(j)} \in \mathbb{R}^L$, $\mathbf{U} \in \mathbb{R}^{L \times J}$, $\mathbf{\mathcal{X}}(\mathbf{x}) \in \mathbb{R}^J$. Here, $\mathbf{U} \times_2^1 \mathbf{\mathcal{X}}(\mathbf{x})$ denotes the tensor contraction operation between the second dimension of tensor \mathbf{U} and the vector (or the first dimension of tensor) $\mathbf{\mathcal{X}}(\mathbf{x})$, while $\mathbf{U} \mathbf{\mathcal{X}}(\mathbf{x})$ is a matrix-vector multiplication. The matrix \mathbf{U} is a stack of nodal values $\mathbf{u}^{(j)}$, while $\mathbf{\mathcal{X}}(\mathbf{x})$ is a vectorized function of \mathbf{x} that is parameterized with nodal coordinates $\mathbf{x}^{(j)}$ in the message passing operation.

The graph node features (i.e., coordinate $(\mathbf{x}^{(j)})$ and value $(\mathbf{u}^{(j)})$) are trainable parameters of the INN. If the nodal coordinates $(\mathbf{x}^{(j)})$ are fixed, one can find nodal values $(\mathbf{u}^{(j)})$ without changing the discretization of the input domain. If the nodal coordinates are also updated, the optimization will adjust the domain discretization similar to r-adaptivity in FEM [21, 22]. Once the forward propagation is defined, the loss function is chosen based on the problem type: training, solving, or calibrating.

Special case 1: regular mesh with Tucker decomposition

When the input domain is discretized with a regular mesh, we can significantly reduce the trainable parameters (or degrees of freedom, DoFs) by leveraging Tensor Decomposition (TD) [13]. One of the widely used TD methods is Tucker decomposition [36, 37]. It approximates a high-order tensor with J_i nodes in i -th dimension as a tensor contraction between dimension-wise matrices and a core tensor \mathbf{G} , which has the same order of the original tensor but with smaller nodes M_i ($< J_i$). The M_i is often called a "mode" to distinguish it from the original node J_i .

Consider a three-input ($I = 3$) and one output ($L = 1$) system and assume the input domain is discretized with $J = J_1 \times J_2 \times J_3$ nodes, as shown in the special case box of Figure 1. To facilitate tensor notation, the nodal values will be denoted with left/right super/sub scripts, ${}_i^m u_l^{(j)}$, where $i \in \mathbb{N}^I$ is the input index, $m \in \mathbb{N}^{M_i}$ is the mode index, $l \in \mathbb{N}^L$ is the output index, and $j \in \mathbb{N}^{J_i}$ is the nodal index.

The interpolated field $\mathcal{J}\mathbf{u}(\mathbf{x}) \in \mathbb{R}^{L=1}$ can be represented as a Tucker product:

$$\mathcal{J}\mathbf{u}(\mathbf{x}) = [\mathbf{G}; (\mathcal{J}_1 \mathbf{u})^T, (\mathcal{J}_2 \mathbf{u})^T, (\mathcal{J}_3 \mathbf{u})^T] = \mathbf{G} \times_1^2 (\mathcal{J}_1 \mathbf{u})^T \times_2^2 (\mathcal{J}_2 \mathbf{u})^T \times_3^2 (\mathcal{J}_3 \mathbf{u})^T, \quad (4)$$

where the core tensor $\mathbf{G} \in \mathbb{R}^{M_1 \times M_2 \times M_3}$ is a trainable full matrix typically smaller than the original tensor that compresses data. The $\mathcal{J}_i \mathbf{u}(x_i) \in \mathbb{R}^{M_i \times 1}$ is one-dimensional (1D) interpolated output of i -th input dimension over M_i modes represented as:

$$\mathcal{J}_i \mathbf{u}(x_i) = \begin{bmatrix} {}_i^1 u^{(1)} & {}_i^1 u^{(2)} & \cdots & {}_i^1 u^{(J_i)} \\ {}_i^2 u^{(1)} & {}_i^2 u^{(2)} & \cdots & {}_i^2 u^{(J_i)} \\ \vdots & \vdots & \vdots & \vdots \\ {}_i^{M_i} u^{(1)} & {}_i^{M_i} u^{(2)} & \cdots & {}_i^{M_i} u^{(J_i)} \end{bmatrix} \cdot \begin{bmatrix} N^{(1)}(x_i) \\ N^{(2)}(x_i) \\ \vdots \\ N^{(J_i)}(x_i) \end{bmatrix} = {}_i \mathbf{U} \times_2^1 {}_i \mathbf{\mathcal{X}}(\mathbf{x}) = {}_i \mathbf{U} {}_i \mathbf{\mathcal{X}}(\mathbf{x}), \quad (5)$$

where ${}_i \mathbf{U} \in \mathbb{R}^{M_i \times J_i}$ and ${}_i \mathbf{\mathcal{X}}(\mathbf{x}) \in \mathbb{R}^{J_i}$. As illustrated in Figure 1's special case box, the message passing (blue arrow) only happens in the axial directions, yielding 1D interpolation functions: $N^{(J_i)}(x_i)$.

When there are more than one outputs ($L > 1$), the interpolated field becomes a vector of L elements:

$$\begin{aligned} \mathcal{J}\mathbf{u}(\mathbf{x}) &= [\mathcal{J}\mathbf{u}_1(\mathbf{x}), \mathcal{J}\mathbf{u}_2(\mathbf{x}), \dots, \mathcal{J}\mathbf{u}_L(\mathbf{x})], \text{ where} \\ \mathcal{J}\mathbf{u}_l(\mathbf{x}) &= [\mathbf{G}_l; (\mathcal{J}_1 \mathbf{u}_l)^T, (\mathcal{J}_2 \mathbf{u}_l)^T, (\mathcal{J}_3 \mathbf{u}_l)^T] = \mathbf{G}_l \times_1^2 (\mathcal{J}_1 \mathbf{u}_l)^T \times_2^2 (\mathcal{J}_2 \mathbf{u}_l)^T \times_3^2 (\mathcal{J}_3 \mathbf{u}_l)^T, \end{aligned} \quad (6)$$

where $\mathcal{J}_i \mathbf{u}_l \in \mathbb{R}^{M_i \times 1}$. The trainable parameters are the core tensors $\mathbf{G}_l \in \mathbb{R}^{M_1 \times M_2 \times M_3}$, $l = 1, \dots, L$, and the nodal values ${}_i \mathbf{U}_l \in \mathbb{R}^{M_i \times J_i}$, $l = 1, \dots, L$, yielding a total count of $L \left(\prod_i^I M_i + \sum_i^I M_i J_i \right)$ that scales linearly with the nodal discretization J_i .

Special case 2: regular mesh with CP decomposition

Tucker decomposition can be further simplified to CANDECOMP/PARAFAC (CP) decomposition [38, 39, 40] by setting the core tensor \mathcal{G} as an order- I super diagonal tensor: $\mathcal{G} \in \mathbb{R}^{M^I}$, $M = M_1 = \dots = M_I$, all zero entries except the diagonal elements. If we further set the diagonal elements of \mathcal{G} to be 1, the Tucker decomposition in Eq. 6 becomes:

$$\mathcal{J}\mathbf{u}(\mathbf{x}) = \sum_{m=1}^M [\mathcal{J}^m \mathbf{u}(x_1) \odot \dots \odot \mathcal{J}^m \mathbf{u}(x_I)], \quad (7)$$

where $\mathcal{J}^m \mathbf{u}(x_i) \in \mathbb{R}^L$ and \odot represents element-wise multiplication. In CP decomposition, the core tensor is no longer trainable, thus the total trainable parameter becomes $ML \sum_i^I J_i$.

It is important to note that the interpolation function $N^{(j)}(x_i)$ in Eq.5 is one-dimensional. In other words, both Tucker and CP decomposition replace a high-dimensional interpolation with one-dimensional interpolations that dramatically reduce the number of trainable parameters (or DoFs). As given in Table 1, the number of trainable parameters of the full interpolation scales exponentially with the discretization J_i , whereas the Tucker and the CP decomposition scale linearly with J_i . Considering the trainable parameters of multi-layer perception (MLP) scales quadratically with the number of hidden neurons, INNs with tensor decomposition (TD) may dramatically reduce the model complexity and computing requirements.

Table 1: Number of trainable parameters (or degrees of freedom, DoFs) of full interpolation, Tucker decomposition, and CP decomposition for an I -input single output ($L = 1$) relationship. The input domain is discretized with a regular grid of $J_1 \times J_2 \times \dots \times J_I$ discretization. We assume that the nodal coordinates ($\mathbf{x}^{(j)}$) are fixed.

	Full interpolation	Tucker decomposition	CP decomposition
Trainable parameters	$\prod_i^I J_i$	$\prod_i^I M_i + \sum_i^I M_i J_i$	$M \sum_i^I J_i$

INN trainer

A general INN forward propagation is provided in Eq.3 as a tensor contraction. The INN trainer optimizes nodal values $\mathbf{U} = \{\mathbf{u}^{(j)}\}_{j=1, \dots, J}$ (and if needed, nodal coordinates $(\mathbf{X} = \{\mathbf{x}^{(j)}\}_{j=1, \dots, J})$) under a given loss function and training data. Consider a regression problem with K labeled data: $(\mathbf{x}_k^*, \mathbf{u}_k^*)$, $k = 1, \dots, K$; and $\mathbf{x}_k^* \in \mathbb{R}^I$, $\mathbf{u}_k^* \in \mathbb{R}^L$. The superscript * denotes data. A mean squared error (MSE) loss function for this regression problem is defined as:

$$\text{loss}(\mathbf{U}, \mathbf{X}) = \frac{1}{K} \sum_k (\mathcal{J}\mathbf{u}(\mathbf{x}_k^*) - \mathbf{u}_k^*)^2. \quad (8)$$

Finally, an optimization is formulated as:

$$\underset{\mathbf{U}, \mathbf{X}}{\text{minimize}} \text{loss}(\mathbf{U}, \mathbf{X}). \quad (9)$$

Section 3.1 exhibits the application of INN trainer to metal additive manufacturing while other benchmarks are elucidated in SI Section 2.

INN solver

An INN solver generalizes classical numerical methods such as FEM and meshfree, as well as the model order reduction methods such as proper generalized decomposition (PGD) [41] and tensor decomposition (TD) [14, 42]. Here, we introduce a formulation with CP decomposition to solve the generalized space (\mathbf{x}) - time (t) - parameter ($\boldsymbol{\theta}$) (S-T-P) PDE, whose computational cost is prohibitively high for most numerical methods and machine learning approaches [41].

Consider a parameterized space-time PDE:

$$\mathcal{L}\mathbf{u}(\mathbf{x}, t, \boldsymbol{\theta}) = 0, \quad (10)$$

where \mathcal{L} is the general partial differential operator (can be linear or nonlinear). The INN solver uses the same neural network structure as the trainer, but the loss function varies with the equations to be solved. It is formulated as the weighted summation of the PDE residual [43, 44, 45]. An INN solution field in the S-T-P domain can be written as:

$$\begin{aligned} \mathcal{J}\mathbf{u}(\mathbf{x}, t, \boldsymbol{\theta}; \mathbf{U}, \mathbf{X}) &= \sum_{m=1}^M [\mathcal{J}_{x_1}^m \mathbf{u}(x_1)] \odot \cdots \odot [\mathcal{J}_{x_d}^m \mathbf{u}(x_d)] \odot [\mathcal{J}_t^m \mathbf{u}(x_t)] \\ &\odot [\mathcal{J}_{\theta_1}^m \mathbf{u}(\theta_1)] \odot \cdots \odot [\mathcal{J}_{\theta_k}^m \mathbf{u}(\theta_k)], \end{aligned} \quad (11)$$

where d and k are the spatial dimension and the number of parameters, respectively. Similar to the trainer, the goal is to find nodal values \mathbf{U} (and nodal coordinates \mathbf{X} , if one wants to adapt the mesh). As a result, the INN obtains the S-T-P solution by minimizing the loss function:

$$\underset{\mathbf{U}, \mathbf{X}}{\text{minimize}} \int \delta \mathbf{u} \cdot \mathcal{L} [\mathcal{J}\mathbf{u}(\mathbf{x}, t, \boldsymbol{\theta}; \mathbf{U}, \mathbf{X})] dx dt d\boldsymbol{\theta}, \quad (12)$$

where $\delta \mathbf{u}$ is the weight function and can be defined using Galerkin, Petrov-Galerkin, collocation or quadratic formulation. Due to the Kronecker delta property of INN interpolation functions, Dirichlet boundary conditions and initial conditions can be strongly imposed. As a result, only the weighted sum residual is considered in Eq. 11 as a loss function. This distinguishes INNs from most data-driven PDE solvers that weakly impose those conditions [46]. See the SI Section 4 for detailed derivations of the loss function and solution scheme. INN solvers applied to the metal additive manufacturing and the linear elastic solid mechanics problem are introduced in Section 3.3 and SI Section 4, respectively.

INN calibrator

The word calibration in mathematics refers to a reverse process of regression, where a known or measured observation of the output variables (\mathbf{u}^*) is used to predict the corresponding input variables (\mathbf{x}^*). By definition, it is analogous to solving an inverse problem in engineering design. To build a good calibrator, having an accurate forward model is of paramount importance, followed by building a good optimizer for the inverse problem. A trained or solved INN has the potential to be a superior candidate for the forward model inside a calibrator because it is fully differentiable and accurate, equipped with fast inference time (\sim milliseconds). A general formulation of the INN calibrator is described below:

$$\mathbf{x}^* = \underset{\mathbf{x}}{\text{argmin}} \frac{1}{K} \sum_k (\mathcal{J}\mathbf{u}(\mathbf{x}) - \mathbf{u}_k^*)^2, \quad (13)$$

where $\mathcal{J}\mathbf{u}(\mathbf{x})$ is the trained or solved forward model, \mathbf{u}_k^* is the k -th measured observation and \mathbf{x}^* is the calibrated input variable. The INN calibrator applied to the heat source calibration task in metal additive manufacturing can be found in Section 3.3 while other benchmarks can be found in SI Section 3.

3 Scientific and Engineering applications: Metal Additive Manufacturing

This section illustrates how Engineering Software 2.0 enabled with INNs can be applied to advance various facets of metal additive manufacturing (AM). Note that the INN with CP decomposition will be referred to as INN in this section for brevity. Laser powder bed fusion (L-PBF) is a type of metal additive manufacturing in which metal powders are layered and melted by a laser beam to create objects that match the provided CAD designs [47]. The added flexibility of L-PBF comes with a huge design space and spatially varying microstructure after manufacturing. Therefore, considerable research is devoted to employing in situ monitoring data for real-time control of L-PBF processes to minimize the variability and optimize the target properties [48]. Computational modeling of L-PBF spans the simulation of the manufacturing process with a high dimensional design space (solving), the identification of model parameters from sparse experimental data (calibrating), and the online monitoring and control of the L-PBF (training).

The governing equation for modeling the manufacturing process is given by a heat conduction equation with a moving laser heat source S_h :

$$\frac{\partial T(\mathbf{x}, t)}{\partial t} - k \Delta T(\mathbf{x}, t) = S_h(\mathbf{x}, t, P, \eta, d) \quad (14)$$

where the equation involves spatial variables \mathbf{x} , temporal variable t , and four variable parameters: thermal conductivity k , laser power P , absorptivity η , and laser depth d . For the simplest case of single track laser pass, the initial condition is $T(\mathbf{x}, 0) = T_0(\mathbf{x})$, and the boundary conditions (BCs) are $T = \bar{T}$ in Γ^D for Dirichlet BC and $\frac{\partial T}{\partial \mathbf{x}} \cdot \mathbf{n} = \bar{q}$ in Γ^N for Neumann BC, where the spatial domain boundary $\Gamma = \Gamma^D \cup \Gamma^N$.

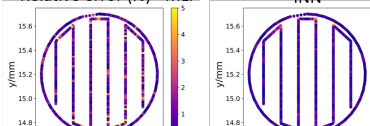
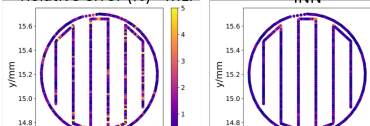
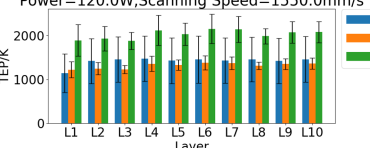
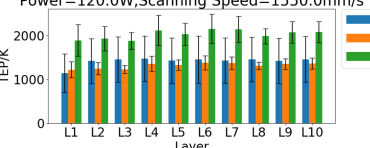
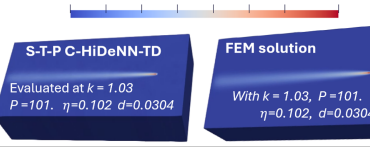
Category	Description	Input/output	Results		Remarks
			Visualization		
Training	Real-time online monitoring of L-PBF process	21 Mechanistic features, thermal field, current laser power (input)/laser power required for the next layer			<ul style="list-style-type: none"> 18 to 31 times faster training than MLP. Requires 82% less trainable parameters than MLP. More accurate prediction than MLP.
Calibration	Heat source parameter calibration	$\text{Depth } d = p_1 \frac{P}{V} RHF^2$ $\text{Absorptivity } \eta = p_2 \frac{P}{V} RHF^2$ $\text{Laser beam radius } r_b = p_3 \frac{P}{V} RHF^2$			<ul style="list-style-type: none"> Very effective for scarce dataset INN: 10^{-4} MSE (100 epoch)/MLP: 10^{-3} MSE (1000 epoch) Relative calibration error: INN 7.9% / MLP 44%
Solving	High-dimensional governing equation for L-PBF	Space-time-parameter inputs (8)/Thermal field			<ul style="list-style-type: none"> No offline data generation required Significant storage gain Accuracy of INN: $R^2 = 0.9969$

Figure 3: A summary of engineering applications of INNs to additive manufacturing (AM) problems. First, a data-driven real-time online monitoring and feedback control tool is formulated with an INN that uses only 18% training parameters of MLP and is 18-31 times faster than MLP. The calibration problem develops a reduced-order model of laser powder bed fusion (L-PBF) AM to calibrate the heat source parameters from experimental data. Finally, the INN solver solves a space-time-parameter heat transfer equation, resulting in a significant storage reduction and faster simulations.

3.1 Real-time Online Control of Laser Powder Bed Fusion Additive Manufacturing

The first application is fully data-driven, where the data are generated from numerical methods and the INN trainer is used to develop an online control system for L-PBF AM. The goal is to maintain a homogeneous temperature of the melt pool (i.e., a molten region near the laser spot) across each layer using real-time sensor data, under the hypothesis that *a homogeneous melt pool temperature across each layer of material deposition will reduce the variability in the microstructure and mechanical properties*. The laser power at each point of a certain layer needs to be controlled (increased/decreased by certain amount compared to previous layer) to achieve this homogeneity in melt pool temperature. The fundamental challenge of implementing a model predictive control system for such an application is the computational resources required for forward prediction (involving finite element or computational fluid dynamics models) and inverse prediction, as illustrated in Figure 3. The INN trainer aims to provide a reliable and memory-efficient surrogate model that can replace mechanistic models in predictive control systems. In this application, the database is generated by fusing experiments and computational methods (see SI Section 2.6 for details) for aluminum alloy. The online control loop uses the trained INN models to inform the manufacturing machine. There are two models: *forward model* and *inverse model*.

The forward model uses the mechanistic features and the thermal emission plank (TEP, a representative of the melt pool temperature) to predict the TEP of the next layer of the build when no correction is applied. The mechanistic features are precomputed based on the tool path and geometry of the build to generalize a data-driven model for unseen tool path and geometric features [49]. The target TEP for the next layer is the average of the forward model's outputs (i.e., predicted TEPs for the next layer) measured at the current layer. The inverse model takes this target TEP as the input along with the previous layer's mechanistic features to predict the required laser power for the next layer. Finally, the control software calculates how much change in laser power is required at each point, and sends the information to the machine. The corrected laser power is then used to print the next layer.

The forward model is trained on experimentally observed data, while the inverse model is trained on computational data coming from a finite-difference solver [18]. The INN model is applied for both forward and inverse prediction and is compared with the MLP. Figure 3 shows that for the inverse model INN is at least 18 to 31 times faster to train compared to the MLP to reach the same level of training error, and it reduced the number of trainable parameters by a

staggering amount of 82%. The speed-up depends on the amount of data used. The INN method is consistently more accurate compared to MLP (see, SI Section 2.6 for more details).

3.2 Calibration of Heat Source Parameters for Additive Manufacturing

In this example, an INN calibrates the heat source function S_h in Eq.14 for experimental data. A Gaussian beam profile is modeled as a volumetric heat source [50], which is written as:

$$S_h(\mathbf{x}, t, \mathbf{p}) = \frac{2P\eta}{\pi r_b^2 d} e^{-\frac{2(x^2+y^2)}{r_b^2}} \cdot \mathbf{1}_{\{z|z_{top}-z \leq d\}}(z) \quad (15)$$

where z_{top} is the z-coordinate of the current surface of the powder bed and $\mathbf{1}$ is the indicator function. The notation follows Eq. 14, and r_b is the Gaussian profile's standard deviation that controls the beam's width. Following reference [10], the heat source parameters d, η, r_b are controlled by the calibration parameters p_1, p_2, p_3 such that $d = p_1 \frac{P}{V} RHF^2$, $\eta = p_2 \frac{P}{V} RHF^2$, and $r_b = p_3 \frac{P}{V} RHF^2$. Here, V is the laser scan speed and RHF is a predetermined residual heat factor based on the laser toolpath [51].

This calibration problem's major challenge is achieving a highly accurate surrogate model given a sparse set of training data. INNs outperform MLPs in solving these data-scarce problems because they are rooted in the interpolation theory. As a demonstration, an INN with 1760 trainable parameters is trained on 28 sets of melt pool temperature data generated by the finite difference method (FDM) [18] using 4 different power-scanning speed set-ups. Later, this trained INN is used as a surrogate to optimize the three parameters (p_1, p_2, p_3) given the experimental data. To show the superiority of INNs over traditional neural networks in such data-scarce applications, a 3-layer MLP with 2689 trainable parameters (roughly the same order of magnitude as the INN) is trained using the same data fed to the INN. In practice, we observed that INN converges well within 100 epoch, while MLP requires over 1000 epoch to converge to a test MSE 10 times larger than INN given all other setup the same. Details on this training and calibration process are provided in SI Section 3.1.

The INN- and MLP-based calibrations are repeated 50 times to provide a statistical comparison (see Figure 3). Even with only 28 sets of simulation data, the calibrated parameters using the INN produce a mean melt pool temperature within a 7.9% difference of the experimental data. In contrast, the parameters calibrated from the MLP surrogate produce a difference of 44. 1%, which is unsatisfactory. This is expected since MLP is a general model requiring a large amount of data to achieve a reliable representation of the problem. On the other hand, the INN achieves a much lower difference, showing that the model can learn underlying physics even with a scarce dataset.

3.3 Solving High Dimensional Space-Time-Parameter Heat Equation

INNs can also be utilized as a solver to directly obtain the surrogate model of the additive manufacturing process involving Space-Time-Parameter (S-T-P) dependencies without generating training data. In this case, an INN is used as a parametric interpolation function in the S-T-P solution space that satisfies the governing physical equation and corresponding boundary conditions. Here, we showcase the power of INN by solving a single-track scan in the L-PBF process. The domain size is 10mm \times 5mm \times 2.5mm with a mesh resolution of 8 μ m. The laser scan speed is 250mm/s. We are interested in obtaining the temperature field which not only depends on space \mathbf{x} and time t but also on the laser and material parameters \mathbf{p} . In other words, the surrogate model f is a mapping from the S-T-P continuum to the temperature field: $f := \mathbb{R}^8 \rightarrow \mathbb{R}$.

The surrogate model f can also be obtained using the classical data-driven approach. In the offline stage, training data can be generated by repeatedly running numerical solvers (such as finite difference method (FDM) and variational multiscale method (VMS)) in the Space-Time domain with different sets of parameters \mathbf{p} . Then a surrogate model is trained with the data. The standard data-driven approach suffers from the curse of dimensionality when the parametric space is high-dimensional. As a result, the data-driven approaches face three challenges at the offline stage: expensive computation for repetitive data generation, huge memory cost for running full-scale simulations, and excessive disk storage of offline training data. We estimate the time and storage required for the data-driven approach with FDM and VMS, as shown in Table 2 and illustrated in Figure 2.

Unlike the data-driven approaches, INN solvers treat the parameters \mathbf{p} as additional parametric inputs. As a result, INNs can directly obtain a parametric surrogate model $f = u(\mathbf{x}, t, \mathbf{p})$ directly from the governing equation without going through the cumbersome offline data generation and surrogate model training process. This is particularly beneficial to high-dimensional parametric surrogate models. Moreover, our results prove the INN solution (or the S-T-P surrogate model) achieves an exceptionally high accuracy of $R^2 = 0.9969$, considering that most data-driven approaches for

Table 2: Performance comparison of different surrogate models. The INN’s discretization in the 4D parametric space is 100^4 , so the corresponding sampling points required for the data-driven methods should be 10^8 . The total simulation time and storage requirement of data-driven approaches are estimated from a single run. Detailed explanations for this benchmark can be found in SI Sections 4.3 and 4.4.

Method	Resolution (μm)	Number of offline simulations	Total offline simulation time	Storage (GB)
Data-driven (FDM)	25	1×10^8	2,600 years	7.82×10^8
Data-driven (VMS)	12.5	1×10^8	9 years	8.79×10^6
INN	8	1	15 minutes	7.37×10^{-2}

S-T-P problems trained on numerical simulation data suffer from low model accuracy, typically below $R^2 = 0.9$ [52]. It is worth mentioning that the physics-informed neural networks (PINNs) can handle the S-T-P problem similar to the INN solver. However, the number of collocation points scales exponentially with the number of inputs, and our preliminary study revealed that PINN fails to converge for the same 8-dimensional S-T-P problem after consuming considerable computational resources (see SI Section 4.4). The performance comparison of INN versus data-driven methods is shown in Table. 2.

4 Conclusions

This article demonstrates that the interpolating neural network (INN) can train, solve, and calibrate scientific and engineering problems that are extremely challenging or prohibitive for existing numerical methods and machine learning models. The keys to INN’s success are 1) it interpolates the graph nodes’ values with well-established interpolation theories (not interpolating training data with a black-box network that often causes overfitting issues) and 2) it leverages the tensor decomposition (TD) to resolve curse of dimensionality. Due to the significantly reduced trainable parameters without losing approximation capabilities, INN can train/solve/calibrate faster with less memory requirement, and achieve extremely high model accuracy and fast inference time.

As this is the original article on INNs, we have myriads of research questions that may gather huge research interests across various areas including but not limited to scientific machine learning, applied mathematics, computer vision, and data science. To mention a few:

- Depending on the problem, INN’s superior training efficiency may cause overfitting issues. The ensemble training (i.e., training on random subsets of the training data) might be a way to enhance the generality of the model for image problems or noisy data.
- Multi-resolution aspect (i.e., a varying number of segments across TD modes) of INNs needs to be investigated. See SI 1.4 for further discussions.
- Similar to the INN solvers, the convergence of INN trainers can be studied mathematically.
- Since INNs can be used as both a solver for physics-based problems and a function approximator for data-driven problems, it is of interest to combine the two behaviors into one single model to solve large-scale problems involving both complex physics and scarce data.
- The superior performance of the INN solver may facilitate multiscale analysis in a vast parametric space. One can integrate the S-T-P INN solver with a concurrent multiscale analysis framework such as self-consistent clustering analysis [53, 54] and open a new direction towards parameterized multiscale analysis.
- The current INN code has been optimized to run on a single GPU. Since the INN forward pass over multiple modes can be parallelized, multi-GPU programming will further speed up the code.
- Although Tucker decomposition has been introduced as a special case 1 in Section 2, the numerical experiments conducted in this article mostly focus on the CP decomposition. Theoretically, Tucker decomposition has a larger approximation space than CP decomposition. Further studies on the numerical aspects of the Tucker decomposition are needed.

We expect INNs will open a next-generation Engineering Software 2.0 that revolutionizes almost all fields of computational science and engineering.

Acknowledgments

We express our sincere gratitude to Dr. Gino Domel, Mr. Joseph P. Leonor, Mr. Stefan Knapik, and Mr. Vispi Karkaria from Northwestern University for their invaluable comments and support throughout this work. We also acknowledge the following grants: DEVCOM Army Research Laboratory under Cooperative Agreement Numbers W911NF-20-2-0292 and W911NF-21-2-02199 to J. Cao and the startup funds provided by Virginia Polytechnic Institute and State University to S. Saha. C. Park acknowledges the internship opportunity with the Freudenberg Group, within the team managed by Dr. Vishwanath Hegadekatte.

References

- [1] A. Karpathy, Software 2.0 (Mar 2017).
URL <https://karpathy.medium.com/software-2-0-a64152b37c35>
- [2] M. Moor, O. Banerjee, Z. S. H. Abad, H. M. Krumholz, J. Leskovec, E. J. Topol, P. Rajpurkar, Foundation models for generalist medical artificial intelligence, *Nature* 616 (7956) (2023) 259–265.
- [3] A. Vaswani, N. Shazeer, N. Parmar, J. Uszkoreit, L. Jones, A. N. Gomez, Ł. Kaiser, I. Polosukhin, Attention is all you need, *Advances in neural information processing systems* 30 (2017).
- [4] L. Lu, P. Jin, G. Pang, Z. Zhang, G. E. Karniadakis, Learning nonlinear operators via deeponet based on the universal approximation theorem of operators, *Nature machine intelligence* 3 (3) (2021) 218–229.
- [5] C. Zhang, A. Shafeeqzadeh, Simulation-free reliability analysis with active learning and physics-informed neural network, *Reliability Engineering & System Safety* 226 (2022) 108716.
- [6] S. Goswami, K. Kontolati, M. D. Shields, G. E. Karniadakis, Deep transfer operator learning for partial differential equations under conditional shift, *Nature Machine Intelligence* 4 (12) (2022) 1155–1164.
- [7] C. Park, Y. Lu, S. Saha, T. Xue, J. Guo, S. Mojumder, D. W. Apley, G. J. Wagner, W. K. Liu, Convolution hierarchical deep-learning neural network (c-hidenn) with graphics processing unit (gpu) acceleration, *Computational Mechanics* (2023) 1–27.
- [8] T. G. Grossmann, U. J. Komorowska, J. Latz, C.-B. Schönlieb, Can physics-informed neural networks beat the finite element method?, *IMA Journal of Applied Mathematics* (2024) hxae011.
- [9] N. McGreivy, A. Hakim, Weak baselines and reporting biases lead to overoptimism in machine learning for fluid-related partial differential equations, *Nature Machine Intelligence* (2024) 1–14.
- [10] A. A. Amin, Y. Li, Y. Lu, X. Xie, Z. Gan, S. Mojumder, G. J. Wagner, W. K. Liu, Physics guided heat source for quantitative prediction of in718 laser additive manufacturing processes, *npj Computational Materials* 10 (37) (2024).
- [11] J. P. Leonor, G. J. Wagner, Go-melt: Gpu-optimized multilevel execution of lpbf thermal simulations, *Computer Methods in Applied Mechanics and Engineering* 426 (2024) 116977.
- [12] M. Shih, K. Chen, T. Lee, D. Tarn, C. Hung, Fe simulation model for warpage evaluation of glass interposer substrate packages, *IEEE Transactions on Components, Packaging and Manufacturing Technology* 11 (4) (2021) 690–696.
- [13] T. G. Kolda, B. W. Bader, Tensor decompositions and applications, *SIAM review* 51 (3) (2009) 455–500.
- [14] L. Zhang, Y. Lu, S. Tang, W. K. Liu, Hidenn-td: Reduced-order hierarchical deep learning neural networks, *Computer Methods in Applied Mechanics and Engineering* 389 (2022) 114414.
- [15] Y. Lu, H. Li, L. Zhang, C. Park, S. Mojumder, S. Knapik, Z. Sang, S. Tang, D. W. Apley, G. J. Wagner, et al., Convolution hierarchical deep-learning neural networks (c-hidenn): finite elements, isogeometric analysis, tensor decomposition, and beyond, *Computational Mechanics* (2023) 1–30.
- [16] H. Li, S. Knapik, Y. Li, C. Park, J. Guo, S. Mojumder, Y. Lu, W. Chen, D. W. Apley, W. K. Liu, Convolution hierarchical deep-learning neural network tensor decomposition (c-hidenn-td) for high-resolution topology optimization, *Computational Mechanics* (2023) 1–20.
- [17] H. Attar, M. Bönisch, M. Calin, L.-C. Zhang, S. Scudino, J. Eckert, Selective laser melting of in situ titanium–titanium boride composites: Processing, microstructure and mechanical properties, *Acta Materialia* 76 (2014) 13–22.
- [18] S. Liao, A. Golgoon, M. Mozaffar, J. Cao, Efficient gpu-accelerated thermomechanical solver for residual stress prediction in additive manufacturing, *Computational Mechanics* 71 (5) (2023) 879–893.

- [19] J. Bradbury, R. Frostig, P. Hawkins, M. J. Johnson, C. Leary, D. Maclaurin, G. Necula, A. Paszke, J. VanderPlas, S. Wanderman-Milne, Q. Zhang, JAX: composable transformations of Python+NumPy programs (2018). URL <http://github.com/jax-ml/jax>
- [20] W. K. Liu, S. Li, H. S. Park, Eighty years of the finite element method: Birth, evolution, and future, *Archives of Computational Methods in Engineering* 29 (6) (2022) 4431–4453.
- [21] L. Zhang, L. Cheng, H. Li, J. Gao, C. Yu, R. Domel, Y. Yang, S. Tang, W. K. Liu, Hierarchical deep-learning neural networks: finite elements and beyond, *Computational Mechanics* 67 (2021) 207–230.
- [22] S. Saha, Z. Gan, L. Cheng, J. Gao, O. L. Kafka, X. Xie, H. Li, M. Tajdari, H. A. Kim, W. K. Liu, Hierarchical deep learning neural network (hidenn): An artificial intelligence (ai) framework for computational science and engineering, *Computer Methods in Applied Mechanics and Engineering* 373 (2021) 113452.
- [23] F. Alet, A. K. Jeewajee, M. B. Villalonga, A. Rodriguez, T. Lozano-Perez, L. Kaelbling, Graph element networks: adaptive, structured computation and memory, in: *International Conference on Machine Learning*, PMLR, 2019, pp. 212–222.
- [24] M. Y. Michelis, R. K. Katschmann, Physics-constrained unsupervised learning of partial differential equations using meshes, *arXiv preprint arXiv:2203.16628* (2022).
- [25] H. Gao, M. J. Zahr, J.-X. Wang, Physics-informed graph neural galerkin networks: A unified framework for solving pde-governed forward and inverse problems, *Computer Methods in Applied Mechanics and Engineering* 390 (2022) 114502.
- [26] T. Xue, Z. Gan, S. Liao, J. Cao, Physics-embedded graph network for accelerating phase-field simulation of microstructure evolution in additive manufacturing, *npj Computational Materials* 8 (1) (2022) 201.
- [27] Z. Wu, S. Pan, F. Chen, G. Long, C. Zhang, S. Y. Philip, A comprehensive survey on graph neural networks, *IEEE transactions on neural networks and learning systems* 32 (1) (2020) 4–24.
- [28] T. J. Hughes, *The finite element method: linear static and dynamic finite element analysis*, Courier Corporation, 2003.
- [29] W. K. Liu, S. Jun, Y. F. Zhang, Reproducing kernel particle methods, *International journal for numerical methods in fluids* 20 (8-9) (1995) 1081–1106.
- [30] T. Belytschko, Y. Y. Lu, L. Gu, Element-free galerkin methods, *International journal for numerical methods in engineering* 37 (2) (1994) 229–256.
- [31] G.-R. Liu, Y.-T. Gu, *An introduction to meshfree methods and their programming*, Springer Science & Business Media, 2005.
- [32] L. Schumaker, *Spline functions: basic theory*, Cambridge university press, 2007.
- [33] T. J. Hughes, J. A. Cottrell, Y. Bazilevs, Isogeometric analysis: Cad, finite elements, nurbs, exact geometry and mesh refinement, *Computer methods in applied mechanics and engineering* 194 (39-41) (2005) 4135–4195.
- [34] T. Strouboulis, K. Cottrell, I. Babuška, The generalized finite element method, *Computer methods in applied mechanics and engineering* 190 (32-33) (2001) 4081–4193.
- [35] R. Tian, Extra-dof-free and linearly independent enrichments in gfem, *Computer Methods in Applied Mechanics and Engineering* 266 (2013) 1–22.
- [36] L. R. Tucker, Implications of factor analysis of three-way matrices for measurement of change, *Problems in measuring change* 15 (122-137) (1963) 3.
- [37] L. R. Tucker, Some mathematical notes on three-mode factor analysis, *Psychometrika* 31 (3) (1966) 279–311.
- [38] R. A. Harshman, et al., Foundations of the parafac procedure: Models and conditions for an “explanatory” multi-modal factor analysis, *UCLA working papers in phonetics* 16 (1) (1970) 84.
- [39] J. D. Carroll, J.-J. Chang, Analysis of individual differences in multidimensional scaling via an n-way generalization of “eckart-young” decomposition, *Psychometrika* 35 (3) (1970) 283–319.
- [40] H. A. Kiers, Towards a standardized notation and terminology in multiway analysis, *Journal of Chemometrics: A Journal of the Chemometrics Society* 14 (3) (2000) 105–122.
- [41] F. Chinesta, P. Ladeveze, E. Cueto, A short review on model order reduction based on proper generalized decomposition, *Archives of Computational Methods in Engineering* 18 (4) (2011) 395–404.
- [42] J. Guo, C. Park, X. Xie, Z. Sang, G. J. Wagner, W. K. Liu, Convolutional hierarchical deep learning neural networks-tensor decomposition (c-hidenn-td): a scalable surrogate modeling approach for large-scale physical systems, *arXiv preprint arXiv:2409.00329* (2024).

- [43] E. Pruliere, F. Chinesta, A. Ammar, On the deterministic solution of multidimensional parametric models using the proper generalized decomposition, *Mathematics and Computers in Simulation* 81 (4) (2010) 791–810.
- [44] E. Kharazmi, Z. Zhang, G. E. Karniadakis, Variational physics-informed neural networks for solving partial differential equations, *arXiv preprint arXiv:1912.00873* (2019).
- [45] E. Kharazmi, Z. Zhang, G. E. Karniadakis, hp-vpinns: Variational physics-informed neural networks with domain decomposition, *Computer Methods in Applied Mechanics and Engineering* 374 (2021) 113547.
- [46] M. Raissi, P. Perdikaris, G. E. Karniadakis, Physics-informed neural networks: A deep learning framework for solving forward and inverse problems involving nonlinear partial differential equations, *Journal of Computational physics* 378 (2019) 686–707.
- [47] V. Bhavar, P. Kattire, V. Patil, S. Khot, K. Gujar, R. Singh, A review on powder bed fusion technology of metal additive manufacturing, *Additive manufacturing handbook* (2017) 251–253.
- [48] Y. Cai, J. Xiong, H. Chen, G. Zhang, A review of in-situ monitoring and process control system in metal-based laser additive manufacturing, *Journal of Manufacturing Systems* 70 (2023) 309–326.
- [49] D. Kozjek, F. M. Carter III, C. Porter, J.-E. Mogonye, K. Ehmann, J. Cao, Data-driven prediction of next-layer melt pool temperatures in laser powder bed fusion based on co-axial high-resolution planck thermometry measurements, *Journal of Manufacturing Processes* 79 (2022) 81–90.
- [50] Y. Li, S. Mojumder, Y. Lu, A. Al Amin, J. Guo, X. Xie, W. Chen, G. J. Wagner, J. Cao, W. K. Liu, Statistical parameterized physics-based machine learning digital shadow models for laser powder bed fusion process, *Additive Manufacturing* 87 (2024) 104214.
- [51] H. Yeung, B. Lane, A residual heat compensation based scan strategy for powder bed fusion additive manufacturing, *Manufacturing letters* 25 (2020) 56–59.
- [52] V. Karkaria, A. Goeckner, R. Zha, J. Chen, J. Zhang, Q. Zhu, J. Cao, R. X. Gao, W. Chen, Towards a digital twin framework in additive manufacturing: Machine learning and bayesian optimization for time series process optimization, *Journal of Manufacturing Systems* (2024).
- [53] Z. Liu, M. Bessa, W. K. Liu, Self-consistent clustering analysis: an efficient multi-scale scheme for inelastic heterogeneous materials, *Computer Methods in Applied Mechanics and Engineering* 306 (2016) 319–341.
- [54] C. Yu, O. L. Kafka, W. K. Liu, Self-consistent clustering analysis for multiscale modeling at finite strains, *Computer Methods in Applied Mechanics and Engineering* 349 (2019) 339–359.